Letter

Current-based metrology with two-terminal mesoscopic conductors

Shishir Khandelwal,[1,2,*] Gabriel T. Landi,[3,4,†] Géraldine Haack,[1,‡] and Mark T. Mitchison[5,6,§]

[1]*Department of Applied Physics, University of Geneva, CH-1211 Geneva, Switzerland*
[2]*Physics Department and NanoLund, Lund University, Box 118, SE-22100 Lund, Sweden*
[3]*Department of Physics and Astronomy, University of Rochester, Rochester, New York 14627, USA*
[4]*University of Rochester Center for Coherence and Quantum Science, Rochester, New York 14627, USA*
[5]*School of Physics, Trinity College Dublin, College Green, Dublin 2, D02 K8N4, Ireland*
[6]*Department of Physics, King's College London, Strand, London WC2R 2LS, United Kingdom*

(Received 22 August 2025; revised 29 September 2025; accepted 2 October 2025; published 24 October 2025)

The traditional approach to quantum parameter estimation focuses on the quantum state, deriving fundamental bounds on precision through the quantum Fisher information. In most experimental settings, however, performing arbitrary quantum measurements is highly unfeasible. In open quantum systems, an alternative approach to metrology involves the measurement of stochastic currents flowing from the system to its environment. However, the present understanding of current-based metrology is mostly limited to Markovian master equations. Considering a parameter estimation problem in a two-terminal mesoscopic conductor, we identify the key elements that determine estimation precision within the Landauer-Büttiker formalism. Crucially, this approach allows us to address arbitrary coupling and temperature regimes. Furthermore, we obtain analytical results for the precision in linear-response and zero-temperature regimes. For the specific parameter estimation task that we consider, we demonstrate that the boxcar transmission function is optimal for current-based metrology in all parameter regimes.

DOI: 10.1103/cpp5-5yw4

Introduction. Quantum parameter estimation is one of the cornerstones of quantum technologies [1] and has been the subject of a wide range of theoretical [2–8] and experimental [9–14] works in recent years. A considerable portion of theoretical research in this area focuses on the quantum state [15,16], through which key statistical quantities such as the quantum Fisher information can be determined. Importantly, this approach sheds light on the fundamental bounds on precision and optimal measurements for quantum metrology. However, achieving optimal precision can require heavily engineered and experimentally unfeasible quantum measurements. This becomes even more challenging in open quantum systems, where environmental noise can reduce the achievable precision and further complicate the identification and implementation of the optimal measurement [17].

In open systems, the measurement of quantum transport observables such as currents is often more feasible. This has motivated systematic statistical analyses of metrology using the output currents of open quantum systems [18]. There are several crucial questions: for example, to determine the key quantities of interest in current-based metrology and to identify the systems and transport conditions that allow for achieving better precision. A strong focus has been on parameter estimation using continuous monitoring of open quantum systems [19], which can often be interpreted as photocurrent-based metrology [20–38]. However, most previous works have focused primarily on optical systems, where the environment can usually be treated within a weak-coupling, Markovian approximation: an assumption that is generally not satisfied in low-temperature transport experiments involving mesoscopic electronic devices.

In this Letter, we address the problem of parameter estimation in two-terminal quantum conductors. In these systems, the electrical current is determined by both the properties of the system and the transport conditions. Therefore, current measurements represent a natural path for parameter estimation. We note that Mihailescu *et al.* [39] recently addressed quantum parameter estimation in mesoscopic electronic setups within an adiabatic linear-response formalism. Here, we focus on precision optimization within the Landauer-Büttiker framework, which holds arbitrarily far from equilibrium so long as interactions between electrons can be neglected (or treated within a mean-field approximation). This approach allows us to determine the optimal conditions for steady-state metrology under arbitrary coupling, voltage bias, and temperature regimes. In this setting, within the linear-response and zero-temperature regimes, we obtain analytical bounds for the precision, identifying and physically interpreting the

*Contact author: shishir.khandelwal@fysik.lu.se
†Contact author: gabriel.landi@rochester.edu
‡Contact author: geraldine.haack@unige.ch
§Contact author: mark.mitchison@kcl.ac.uk

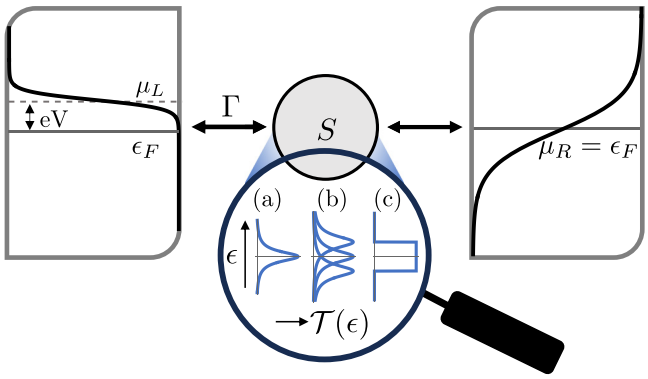

FIG. 1. A two-terminal mesoscopic conductor embedded between two fermionic leads. The energy bias eV provided by the bias voltage pushes the system out of equilibrium. The transport properties depend on the transmission function $\mathcal{T}(\epsilon)$; we consider (a) Lorentzian, (b) sums of Lorentzians, and (c) boxcar shapes.

fundamental elements that determine precision in current-based metrology. We also demonstrate numerically that the optimal transmission function for current-based metrology is the boxcar function (i.e., energy-independent transmission within a given window) (see Fig. 1), both within and far beyond the linear-response regime.

Current-based metrology. We consider the two-terminal setup shown in Fig. 1, with a device embedded between two fermionic reservoirs indexed by $\alpha = L, R$. As the mesoscopic device, we consider a two-terminal conductor which, within a scattering approach to transport, is fully characterized by its energy-dependent transmission function $\mathcal{T}(\epsilon)$. The reservoir modes are characterized by their temperatures T_α and chemical potentials μ_α. We consider thermal equilibrium corresponding to $T_L = T_R \equiv T$ and a finite bias voltage V. The energy bias between the two contacts is given by eV with respect to the Fermi energy of the two contacts, ϵ_F, i.e., $\mu_L = \epsilon_F + eV$ and $\mu_R = \epsilon_F$. This bias sets up a steady-state current I flowing through the system.

Our goal is to establish how well a current measurement can be used to infer some parameter θ of the underlying system. In principle, θ may be a property of the reservoirs (for example, the temperature) or the system (for example, the energy of a quantum dot). We assume the current is measured by integrating the signal from an ammeter over a time window τ. This is equivalent to measuring the charge Q transferred into one of the reservoirs (say, $\alpha = R$), which can be modeled by a two-point measurement of the electron number in the same reservoir [40]. At long times, the mean $\langle Q\rangle$ and variance $\mathrm{Var}[Q]$ are related to the statistics of the current as $\langle Q\rangle = \tau\langle I\rangle$ and $\mathrm{Var}[Q] = \tau\langle\langle I^2\rangle\rangle$, where $\langle I\rangle$ is the mean steady-state current and $\langle\langle I^2\rangle\rangle$ is the dc current noise or diffusion coefficient. As shown in the Supplemental Material (SM) Sec. A [41] (see also Ref. [42]), these relations hold for $\tau \gg t_{\mathrm{rel}}, t_{\mathrm{cor}}$, where t_{rel} is the relaxation time to the steady state and t_{cor} is the decay time of the current-current autocorrelation function.

We focus on local parameter estimation, where the unknown parameter θ lies close to some known value θ_0, and assume that the mean charge $\langle Q\rangle = \Phi(\theta)$ is a known, differentiable function of θ in the vicinity of θ_0. Then, it is easy to check that the estimator $\check{\theta} = \theta_0 + [Q - \Phi(\theta_0)]/\Phi'(\theta_0)$ is locally unbiased, i.e. $\langle\check{\theta}\rangle = \theta + O[(\theta - \theta_0)^2]$, and has a variance given by $\mathrm{Var}[\check{\theta}] = \mathrm{Var}[Q]/(\partial_\theta\langle Q\rangle)^2 = (\gamma\tau)^{-1}$, where the *precision rate* is defined by

$$\gamma = \frac{(\partial_\theta\langle I\rangle)^2}{\langle\langle I^2\rangle\rangle}. \tag{1}$$

That is, the estimation error falls linearly in the time of charge measurement, with a rate given by Eq. (1). As discussed in SM Sec. B [41], γ is upper bounded by the Fisher-information rate and this bound is saturated whenever the distribution of Q is Gaussian, as expected at long times by the central-limit theorem [43]. Both $\langle I\rangle$ and $\langle\langle I^2\rangle\rangle$ have exact expressions within Landauer-Büttiker theory [44,45], which are quoted explicitly in SM Sec. C [41]. In the following, we use these expressions to analyze the estimation precision of current-based metrology in two-terminal devices.

Linear response at thermal equilibrium. At thermal equilibrium, in the linear-response regime for the charge current, $eV \ll k_BT, \epsilon_F$, the current and noise are set by the conductance $G = -2\frac{e^2}{h}\int d\epsilon\mathcal{T}(\epsilon)\partial_\epsilon f(\epsilon, T)$, $\langle I\rangle_{\mathrm{LR}} = GV$, and $\langle\langle I^2\rangle\rangle_{\mathrm{LR}} = 4k_BTG$ [45]. The precision rate γ from Eq. (1) can therefore be expressed as

$$\gamma_{\mathrm{LR}} = \frac{V^2(\partial_\theta G)^2}{4k_BTG} = \frac{1}{4}\frac{eV}{k_BT}(\partial_\theta \ln G)^2\frac{GV}{e}. \tag{2}$$

This result enables a clear interpretation of the sensitivity of a two-terminal mesoscopic conductor. The first factor on the right-hand side is a dimensionless ratio that characterizes the (inverse) scale of thermal fluctuations set by the energy transport window eV and the thermal energy k_BT. The second factor captures the relative sensitivity to the parameter θ, represented by the logarithmic derivative of the conductance, which is a property of the conductor. Finally, the last factor GV/e corresponds to the particle current, i.e., the rate at which the charge is measured. Equation (2) is valid both when the parameter to be estimated is a property of the conductor (for example, the bare energy of a quantum dot) or a property of the reservoirs (for example, the temperature).

Zero-temperature limit. At zero temperature, the Fermi distributions behave as Heaviside functions, $f_\alpha(\epsilon) \equiv \Theta(\mu_\alpha - \epsilon)$. This sets a finite energy window of width eV through which charge transport takes place. In general, this limit entails full (nonlinear) response in the bias voltage. Therefore, full Landauer-Büttiker expressions for current and noise must be considered to calculate the precision. As shown in the Supplemental Material [41], the zero-temperature precision then takes the form

$$\gamma_0 = \frac{1}{h}\frac{\left(\int_{\epsilon_F}^{\epsilon_F+eV} d\epsilon\partial_\theta\mathcal{T}(\epsilon)\right)^2}{\int_{\epsilon_F}^{\epsilon_F+eV} d\epsilon\mathcal{T}(\epsilon)[1-\mathcal{T}(\epsilon)]}. \tag{3}$$

Naturally, to have a nontrivial parameter estimation, θ must now be a property of the conductor, entering its transmission function $\mathcal{T}(\epsilon)$. Approximating γ_0 within the linear-response regime permits further analytical insights. As explained in detail in SM Sec. C [41], linear response at zero temperature corresponds to weak energy dependence of the transmission function over the bias window, permitting the Sommerfeld

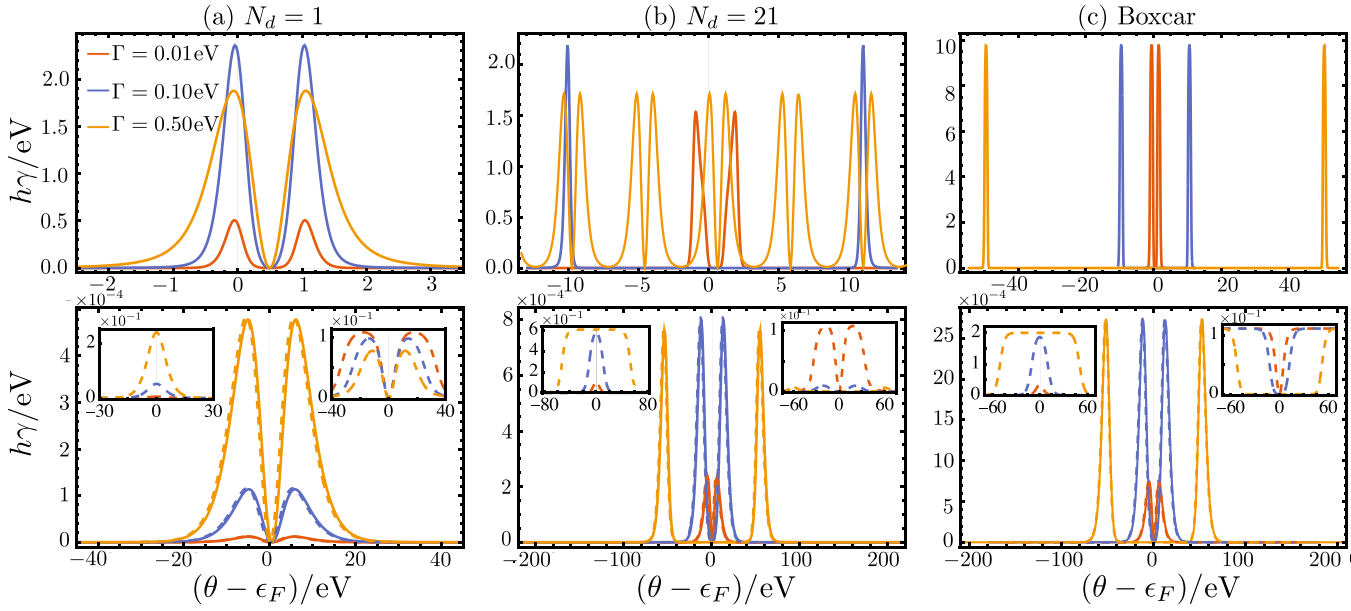

FIG. 2. Precision rate γ as a function of θ, (a) single Lorentzian, $N = 1$, (b) $N = 21$, and (c) boxcar transmission function for $k_BT = 0.1$ eV (top) and $k_BT = 3$ eV (bottom), and three values of $\Gamma = 0.01, 0.1, 0.5$ eV. Solid curves have been drawn with full Landauer-Büttiker expressions and dashed with the linear-response expression (2). In all bottom panels, the left inset shows the conductance as a function of θ and the right, relative sensitivity. $\delta = 100\Gamma$ is set throughout the figure.

expansion $\mathcal{T}(\epsilon) \approx \mathcal{T}_F + (\epsilon - \epsilon_F)\partial_\epsilon \mathcal{T}(\epsilon)|_{\epsilon=\epsilon_F}$, where $\mathcal{T}_F \equiv \mathcal{T}(\epsilon_F)$ is the transmission function evaluated at the Fermi energy. With this expansion, the current and noise are given by $\langle I\rangle_{\rm LR}^{T\to 0} = (2e^2V/h)\mathcal{T}_F$ and $\langle\langle I^2\rangle\rangle_{\rm LR}^{T\to 0} = (4e^3V/h)\mathcal{T}_F(1-\mathcal{T}_F)$, respectively. Therefore, the following expression for the precision rate is obtained,

$$\gamma_0 = \frac{eV\mathcal{T}_F(\partial_\theta \ln \mathcal{T}_F)^2}{h(1-\mathcal{T}_F)} = \frac{1}{2}\frac{\mathcal{T}_F}{1-\mathcal{T}_F}(\partial_\theta \ln \mathcal{T}_F)^2\frac{G_0V}{e}, \quad (4)$$

where $G_0 = 2e^2/h$ is the quantum of conductance. This expression has an elegant interpretation: Each electron transmitted across the junction can be considered as a successful Bernoulli trial, with $\mathcal{T}_F$ the success probability. The first factor $\mathcal{T}_F/(1-\mathcal{T}_F)$ is then the signal-to-noise ratio (the mean squared divided by the variance) of the Bernoulli random variable. Under our assumption that $\mathcal{T}_F$ is approximately energy independent, the conductance is $G = G_0\mathcal{T}_F$, so that the second factor is the relative sensitivity as seen also in Eq. (2). Finally, G_0V/e represents the frequency with which the Bernoulli trials are attempted.

Lorentzian transmission function. To illustrate the general formulas derived above, we first consider the specific example of a two-terminal quantum conductor with a Lorentzian transmission function,

$$\mathcal{T}^{\rm lor}(\epsilon) = \frac{\Gamma^2}{\Gamma^2 + (\theta-\epsilon)^2}. \quad (5)$$

This corresponds to a single-level quantum dot with energy θ. The coupling Γ characterizes the width, with 2Γ the full width at half maximum.

In Fig. 2(a), we show the precision rate as a function of θ computed with both the exact Landauer-Büttiker expressions (solid curves) and the linear-response result (dashed curves). Naturally, the linear-response approximation breaks down for $k_BT \lesssim eV$, so it is only displayed for the high-temperature regime shown in the bottom panel. Due to the form of the transmission function, the curves are symmetric around a local minimum, showing two equal peaks. Insets in the bottom panel of Fig. 2(a) show the conductance (left) and the relative sensitivity (right) in linear response. At larger coupling, the increase in conductance compensates for the lowering of the relative sensitivity, leading to higher precision. Beyond linear response, at low temperature [top panel of Fig. 2(a)], the precision rate is sharply peaked near $\theta = \mu_{L,R}$ and its maximum value is up to four orders of magnitude greater than in the linear-response regime.

The zero-temperature limit (4) with a Lorentzian transmission function takes the following simple form,

$$\gamma_0 = 2\frac{G_0V}{e}\left(\frac{\mathcal{T}_F^{\rm lor}}{\Gamma}\right)^2. \quad (6)$$

The maximum $\gamma_0^{\rm max} = 2G_0V/(\Gamma^2 e)$ lies at $\theta = \epsilon_F$. It can be checked that the above corresponds to the expansion of Eq. (3) with a Lorentzian transmission function to lowest order in eV/Γ. Therefore, the approximation of smooth energy dependence for a Lorentzian transmission function implicitly corresponds to the strong-coupling regime $eV \ll \Gamma$ between the conductor (the dot) and the reservoirs.

Multiple Lorentzians and the boxcar transmission function. We now consider a boxcar transmission function,

$$\mathcal{T}^{\rm box}(\epsilon) = \Theta(\epsilon + \delta - \theta) - \Theta(\epsilon - \delta - \theta), \quad (7)$$

where 2δ is the width of $\mathcal{T}^{\rm box}$ and θ represents an overall energy translation in the positive direction. As shown in SM Sec. D [41], this transmission function can be seen as arising as a sum of sharply peaked Lorentzians under a certain limit.

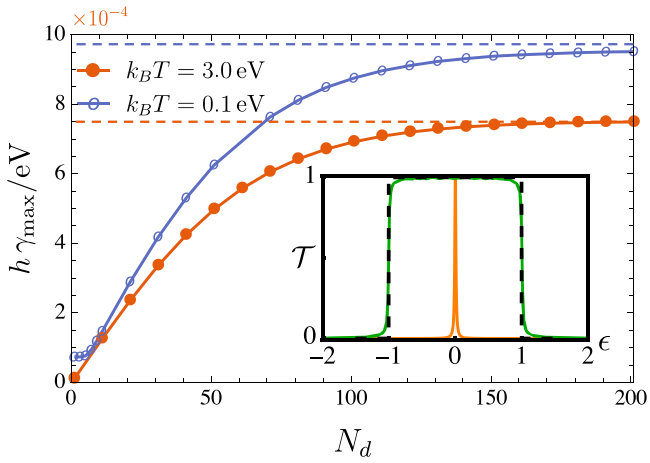

FIG. 3. The maximum precision $\gamma_{\max}$ (optimized over θ) obtained with the full Landauer-Büttiker expressions, as a function of the number of Lorenztians N added within the energy window $[-\delta, \delta]$. The dashed lines are obtained with a boxcar transmission function over the same energy window. Parameters: $k_BT = 3$ eV, $\delta = 100\Gamma$. The inset shows $\mathcal{T}^{\mathrm{box}}$ (dashed, black), a $\mathcal{T}^{\mathrm{lor}}$ (orange), and $\mathcal{T}_N$ with $N_d = 201$ (green).

This allows us to build a smooth approximation for the boxcar by placing $N + 1$ Lorentzians with width Γ, centered at evenly spaced points in the energy window $[-\delta, \delta]$, and appropriately normalizing the sum. This corresponds to the transmission function of $N_d = N + 1$ quantum dots,

$$\mathcal{T}_N(\epsilon) = \frac{1}{\mathcal{N}} \sum_{i=0}^{N_d-1} \frac{\Gamma^2}{\Gamma^2 + (\epsilon_i - \epsilon)}, \tag{8}$$

where $\epsilon_i = -\delta + i\Delta$ is the median of Lorentzian i, $\Delta = 2\delta/(N_d - 1)$, and $\mathcal{N} = \sum_{i=0}^{N_d-1} \Gamma^2/(\Gamma^2 + \epsilon_i^2)$. While this function does not produce a boxcar exactly, in the regimes $\Gamma \ll \delta$ and $N_d \gg \delta/\Gamma$, it provides a reasonable approximation; see the inset of Fig. 3 for an illustration and SM Sec. D for details [41].

We now compare the precision obtained in the case of a single Lorentzian transmission function with that obtained with a sum of many such functions and the boxcar function of Eq. (8). In Figs. 2(b) and 2(c), we show the precision rate as a function of θ in the case of multiple (specifically, a sum of 21) Lorentzians and a boxcar transmission function, within the same energy window $[-\delta, \delta]$, respectively. Note that we have appropriately normalized this energy such that $\delta = 100\Gamma$ is held constant. This is necessary to ensure a smooth approximation to the boxcar function in the limit of large N_d, and to make a fair comparison with the boxcar case. While the general behaviors are often similar in the three cases, the precision rate in the case of $\mathcal{T}_N$ can show more than two peaks. In all coupling and temperature regimes, we find an increase in the precision rate for $\mathcal{T}_N$, and even further for $\mathcal{T}^{\mathrm{box}}$, as compared to the single Lorentzian case.

To assess how precision depends on the shape of the transmission function, we vary N_d to smoothly interpolate between a sharply peaked (Lorentzian) and a flat (boxcar) transmission function. For each value of N_d, we compute the optimal precision rate (maximized over θ) and plot the results in Fig. 3 for two different temperatures. These temperatures are chosen such that the red curve corresponds to the linear-response regime ($eV \ll k_BT$), whereas the blue curve is far away from it. We again choose $\Gamma \ll \delta$ to simulate a boxcar as precisely as possible at large N_d. This is necessary to ensure that the solid curves obtained with $\mathcal{T}_N$ almost match with the dashed curves obtained with the boxcar. At both temperatures considered in Fig. 3, the precision rate increases monotonically with N_d, saturating to the maximum value as $\mathcal{T}_N$ approaches a boxcar function at large N_d. Interestingly, moreover, we show in SM Sec. E [41] that the precision rate for the boxcar function diverges at zero temperature, originating from a diverging signal-to-noise ratio in this situation. From this investigation, we conclude that the boxcar transmission function is optimal for current-based parameter estimation in two-terminal mesoscopic conductors within and beyond the linear-response regime at any temperature.

Conclusion. In this Letter, we have formulated precision bounds within a Landauer-Büttiker formalism, allowing to assess metrology limits in two-terminal quantum coherent conductors. Analytical expressions are derived in two limits, at thermal equilibrium [Eq. (2)] and at zero temperature [Eq. (4)]. These results enable a transparent understanding of the key parameters and energy scales for optimization of the precision rate. In addition, we compare current-based metrology between different transmission functions, interpolating between a single-peak Lorentzian and a boxcar function. Our results indicate that, in the linear-response regime, strong coupling enhances precision by boosting sensitivity, while outside of the linear response we find that intermediate-coupling strengths $\Gamma \sim k_BT$ are optimal. Meanwhile, low temperature is generally beneficial because it suppresses current noise. Furthermore, we numerically find that the boxcar transmission function is optimal for parameter estimation in quantum coherent mesoscopic conductors, in all parameter regimes considered. Interestingly, boxcar transmission functions have been found to be optimal for the efficiency [46,47] and constancy [48] of thermoelectric power generation in similar setups. Such an energy-independent transmission probability can be approximated by a linear chain of quantum dots with carefully engineered couplings [49]. This has been shown to be possible with only a small number of dots with tunnel couplings and site energies inhomogeneously tuned [50]. Control over the individual potential landscape of linear quantum-dot arrays with $N_d \sim 10$ has been achieved [51]. While further scalability is an issue, machine-learning techniques for automated device control could be exploited to overcome this challenge in experiments [52].

While our exact analysis within the Landauer-Büttiker formalism enabled optimization of precision across arbitrary regimes of coupling strength and nonequilibrium bias, this approach neglects interactions between charge carriers. Our results therefore complement those of Ref. [39], which derived the quantum Fisher information for interacting systems within adiabatic linear-response theory, thus assuming weak deviation from equilibrium. We also emphasize that our precision analysis is restricted to a specific, accessible observable: the charge current. This is readily measured in experiments but it may not be an optimal observable in the metrological

sense of saturating the quantum Cramér-Rao bound [15]. An interesting future research problem is thus to find the optimal precision in far-from-equilibrium settings, as dictated by the quantum Fisher information of the entire system-reservoir setup, and establish whether it can be achieved by realistic measurements. Since currents are defined by measurements at (at least) two times, this calls for an inherently multitime approach beyond the Markov approximation, e.g., as in Refs. [22,24,53]. This may shed light on whether nonequilibrium steady-state entanglement [54–58] or quantum violations of classical precision bounds [50,59–67] can provide further advantages for current-based metrology.

Acknowledgments. We thank Gianmichele Blasi, George Mihailescu, Andrew K. Mitchell, and Patrick P. Potts for insightful discussions. S.K. acknowledges support from the Swiss National Science Foundation Grant No. P500PT_-222265 and the Knut and Alice Wallenberg Foundation through the Wallenberg Center for Quantum Technology (WACQT). G.H. acknowledges financial support from the NCCR SwissMAP from the Swiss National Science Foundation. M.T.M. is supported by a Royal Society University Research Fellowship. This project is co-funded by the European Union (Quantum Flagship project ASPECTS, Grant Agreement No. 101080167) and U.K. Research & Innovation (UKRI). Views and opinions expressed are however those of the authors only and do not necessarily reflect those of the European Union, Research Executive Agency or UKRI. Neither the European Union nor UKRI can be held responsible for them. G.T.L. is supported by the U.S. Department of Energy (DOE), Office of Science, Basic Energy Sciences (BES) under Award No. DE-SC0025516.

Data availability. The data that support the findings of this article are not publicly available. The data are available from the authors upon reasonable request.

[1] V. Giovannetti, S. Lloyd, and L. Maccone, Advances in quantum metrology, Nat. Photonics **5**, 222 (2011).
[2] S. Alipour, M. Mehboudi, and A. T. Rezakhani, Quantum metrology in open systems: Dissipative Cramér-Rao bound, Phys. Rev. Lett. **112**, 120405 (2014).
[3] M. Mehboudi, A. Lampo, C. Charalambous, L. A. Correa, M. A. García-March, and M. Lewenstein, Using polarons for sub-nK quantum nondemolition thermometry in a Bose-Einstein condensate, Phys. Rev. Lett. **122**, 030403 (2019).
[4] M. T. Mitchison, T. Fogarty, G. Guarnieri, S. Campbell, T. Busch, and J. Goold, *In situ* thermometry of a cold Fermi gas via dephasing impurities, Phys. Rev. Lett. **125**, 080402 (2020).
[5] M. Perarnau-Llobet, A. González-Tudela, and J. I. Cirac, Multimode Fock states with large photon number: Effective descriptions and applications in quantum metrology, Quantum Sci. Technol. **5**, 025003 (2020).
[6] M. Perarnau-Llobet, D. Malz, and J. I. Cirac, Weakly invasive metrology: Quantum advantage and physical implementations, Quantum **5**, 446 (2021).
[7] R. Salvia, M. Mehboudi, and M. Perarnau-Llobet, Critical quantum metrology assisted by real-time feedback control, Phys. Rev. Lett. **130**, 240803 (2023).
[8] P. Abiuso, P. Sekatski, J. Calsamiglia, and M. Perarnau-Llobet, Fundamental limits of metrology at thermal equilibrium, Phys. Rev. Lett. **134**, 010801 (2025).
[9] W. Wang, Y. Wu, Y. Ma, W. Cai, L. Hu, X. Mu, Y. Xu, Z.-J. Chen, H. Wang, Y. P. Song, H. Yuan, C. L. Zou, L. M. Duan, and L. Sun, Heisenberg-limited single-mode quantum metrology in a superconducting circuit, Nat. Commun. **10**, 4382 (2019).
[10] R. Liu, Y. Chen, M. Jiang, X. Yang, Z. Wu, Y. Li, H. Yuan, X. Peng, and J. Du, Experimental critical quantum metrology with the Heisenberg scaling, npj Quantum Inf. **7**, 170 (2021).
[11] C. D. Marciniak, T. Feldker, I. Pogorelov, R. Kaubruegger, D. V. Vasilyev, R. van Bijnen, P. Schindler, P. Zoller, R. Blatt, and T. Monz, Optimal metrology with programmable quantum sensors, Nature (London) **603**, 604 (2022).
[12] X. Long, W.-T. He, N.-N. Zhang, K. Tang, Z. Lin, H. Liu, X. Nie, G. Feng, J. Li, T. Xin, Q. Ai, and D. Lu, Entanglement-enhanced quantum metrology in colored noise by quantum Zeno effect, Phys. Rev. Lett. **129**, 070502 (2022).
[13] P. Yin, X. Zhao, Y. Yang, Y. Guo, W.-H. Zhang, G.-C. Li, Y.-J. Han, B.-H. Liu, J.-S. Xu, G. Chiribella, G. Chen, C.-F. Li, and G.-C. Guo, Experimental super-Heisenberg quantum metrology with indefinite gate order, Nat. Phys. **19**, 1122 (2023).
[14] M. Valeri, V. Cimini, S. Piacentini, F. Ceccarelli, E. Polino, F. Hoch, G. Bizzarri, G. Corrielli, N. Spagnolo, R. Osellame, and F. Sciarrino, Experimental multiparameter quantum metrology in adaptive regime, Phys. Rev. Res. **5**, 013138 (2023).
[15] M. G. A. Paris, Quantum estimation for quantum technology, Int. J. Quantum Inf. **07**, 125 (2009).
[16] G. Tóth and I. Apellaniz, Quantum metrology from a quantum information science perspective, J. Phys. A: Math. Theor. **47**, 424006 (2014).
[17] J. F. Haase, A. Smirne, S. F. Huelga, J. Kołodynski, and R. Demkowicz-Dobrzanski, Precision limits in quantum metrology with open quantum systems, Quantum Meas. Quantum Metrol. **5**, 13 (2016).
[18] G. T. Landi, M. J. Kewming, M. T. Mitchison, and P. P. Potts, Current fluctuations in open quantum systems: Bridging the gap between quantum continuous measurements and full counting statistics, PRX Quantum **5**, 020201 (2024).
[19] H. Mabuchi, Dynamical identification of open quantum systems, Quantum Semiclassical Opt. **8**, 1103 (1996).
[20] J. Gambetta and H. M. Wiseman, State and dynamical parameter estimation for open quantum systems, Phys. Rev. A **64**, 042105 (2001).
[21] J. K. Stockton, J. M. Geremia, A. C. Doherty, and H. Mabuchi, Robust quantum parameter estimation: Coherent magnetometry with feedback, Phys. Rev. A **69**, 032109 (2004).
[22] M. Tsang, H. M. Wiseman, and C. M. Caves, Fundamental quantum limit to waveform estimation, Phys. Rev. Lett. **106**, 090401 (2011).
[23] J. F. Ralph, K. Jacobs, and C. D. Hill, Frequency tracking and parameter estimation for robust quantum state estimation, Phys. Rev. A **84**, 052119 (2011).

[24] M. Tsang, Quantum metrology with open dynamical systems, New J. Phys. **15**, 073005 (2013).

[25] S. Gammelmark and K. Mølmer, Bayesian parameter inference from continuously monitored quantum systems, Phys. Rev. A **87**, 032115 (2013).

[26] A. H. Kiilerich and K. Mølmer, Estimation of atomic interaction parameters by photon counting, Phys. Rev. A **89**, 052110 (2014).

[27] C. Catana, L. Bouten, and M. Guţă, Fisher informations and local asymptotic normality for continuous-time quantum Markov processes, J. Phys. A: Math. Theor. **48**, 365301 (2015).

[28] K. Macieszczak, M. Guţă, I. Lesanovsky, and J. P. Garrahan, Dynamical phase transitions as a resource for quantum enhanced metrology, Phys. Rev. A **93**, 022103 (2016).

[29] S. Ng, S. Z. Ang, T. A. Wheatley, H. Yonezawa, A. Furusawa, E. H. Huntington, and M. Tsang, Spectrum analysis with quantum dynamical systems, Phys. Rev. A **93**, 042121 (2016).

[30] F. Albarelli, M. A. C. Rossi, M. G. A. Paris, and M. G. Genoni, Ultimate limits for quantum magnetometry via time-continuous measurements, New J. Phys. **19**, 123011 (2017).

[31] F. Albarelli, M. A. C. Rossi, D. Tamascelli, and M. G. Genoni, Restoring Heisenberg scaling in noisy quantum metrology by monitoring the environment, Quantum **2**, 110 (2018).

[32] L. A. Clark, A. Stokes, and A. Beige, Quantum jump metrology, Phys. Rev. A **99**, 022102 (2019).

[33] M. A. C. Rossi, F. Albarelli, D. Tamascelli, and M. G. Genoni, Noisy quantum metrology enhanced by continuous nondemolition measurement, Phys. Rev. Lett. **125**, 200505 (2020).

[34] T. Ilias, D. Yang, S. F. Huelga, and M. B. Plenio, Criticality-enhanced quantum sensing via continuous measurement, PRX Quantum **3**, 010354 (2022).

[35] M. Tsang, Quantum noise spectroscopy as an incoherent imaging problem, Phys. Rev. A **107**, 012611 (2023).

[36] D. Yang, S. F. Huelga, and M. B. Plenio, Efficient information retrieval for sensing via continuous measurement, Phys. Rev. X **13**, 031012 (2023).

[37] A. Godley and M. Guta, Adaptive measurement filter: Efficient strategy for optimal estimation of quantum Markov chains, Quantum **7**, 973 (2023).

[38] A. Cabot, F. Carollo, and I. Lesanovsky, Continuous sensing and parameter estimation with the boundary time crystal, Phys. Rev. Lett. **132**, 050801 (2024).

[39] G. Mihailescu, A. Kiely, and A. K. Mitchell, Quantum sensing with nanoelectronics: Fisher information for an adiabatic perturbation, arXiv:2406.18662.

[40] M. Esposito, U. Harbola, and S. Mukamel, Nonequilibrium fluctuations, fluctuation theorems, and counting statistics in quantum systems, Rev. Mod. Phys. **81**, 1665 (2009).

[41] See Supplemental Material at http://link.aps.org/supplemental/10.1103/cpp5-5yw4 for detailed derivations of all the results in the manuscript, which also contains Refs. [42,44].

[42] S. M. Kay, *Fundamentals of Statistical Signal Processing. 1: Estimation Theory*, 20th ed. (Prentice Hall, Hoboken, NJ, 2013).

[43] In fact, Eq. (1) can also be derived from a saddle-point approximation of the charge characteristic function as $\tau \to \infty$ (e.g., see Sec. V E of Ref. [18]), without any explicit Gaussian assumption. We thank Patrick P. Potts for pointing this out to us.

[44] M. Büttiker, Scattering theory of current and intensity noise correlations in conductors and wave guides, Phys. Rev. B **46**, 12485 (1992).

[45] Y. Blanter and M. Büttiker, Shot noise in mesoscopic conductors, Phys. Rep. **336**, 1 (2000).

[46] R. S. Whitney, Most efficient quantum thermoelectric at finite power output, Phys. Rev. Lett. **112**, 130601 (2014); Finding the quantum thermoelectric with maximal efficiency and minimal entropy production at given power output, Phys. Rev. B **91**, 115425 (2015).

[47] L. Tesser, R. S. Whitney, and J. Splettstoesser, Thermodynamic performance of hot-carrier solar cells: A quantum transport model, Phys. Rev. Appl. **19**, 044038 (2023).

[48] A. M. Timpanaro, G. Guarnieri, and G. T. Landi, Quantum thermoelectric transmission functions with minimal current fluctuations, Phys. Rev. B **111**, 014301 (2025).

[49] T. Ehrlich and G. Schaller, Broadband frequency filters with quantum dot chains, Phys. Rev. B **104**, 045424 (2021).

[50] K. Brandner and K. Saito, Thermodynamic uncertainty relations for coherent transport, Phys. Rev. Lett. **135**, 046302 (2025).

[51] A. R. Mills, D. M. Zajac, M. J. Gullans, F. J. Schupp, T. M. Hazard, and J. R. Petta, Shuttling a single charge across a one-dimensional array of silicon quantum dots, Nat. Commun. **10**, 1063 (2019).

[52] J. P. Zwolak and J. M. Taylor, *Colloquium:* Advances in automation of quantum dot devices control, Rev. Mod. Phys. **95**, 011006 (2023).

[53] G. Blasi, S. Khandelwal, and G. Haack, Exact finite-time correlation functions for multiterminal setups: Connecting theoretical frameworks for quantum transport and thermodynamics, Phys. Rev. Res. **6**, 043091 (2024).

[54] S. Khandelwal, N. Palazzo, N. Brunner, and G. Haack, Critical heat current for operating an entanglement engine, New J. Phys. **22**, 073039 (2020).

[55] D. Heineken, K. Beyer, K. Luoma, and W. T. Strunz, Quantum-memory-enhanced dissipative entanglement creation in nonequilibrium steady states, Phys. Rev. A **104**, 052426 (2021).

[56] G. F. Diotallevi, B. Annby-Andersson, P. Samuelsson, A. Tavakoli, and P. Bakhshinezhad, Steady-state entanglement production in a quantum thermal machine with continuous feedback control, New J. Phys. **26**, 053005 (2024).

[57] L. Mortimer, D. Farina, G. D. Bello, D. Jansen, A. Leitherer, P. Mujal, and A. Acín, Certifying steady-state properties of open quantum systems, Phys. Rev. Res. **7**, 033237 (2025).

[58] S. Khandelwal, B. Annby-Andersson, G. F. Diotallevi, A. Wacker, and A. Tavakoli, Maximal steady-state entanglement in autonomous quantum thermal machines, npj Quantum Inf. **11**, 28 (2025).

[59] K. Ptaszyński, Coherence-enhanced constancy of a quantum thermoelectric generator, Phys. Rev. B **98**, 085425 (2018).

[60] K. Brandner, T. Hanazato, and K. Saito, Thermodynamic bounds on precision in ballistic multiterminal transport, Phys. Rev. Lett. **120**, 090601 (2018).

[61] G. Guarnieri, G. T. Landi, S. R. Clark, and J. Goold, Thermodynamics of precision in quantum nonequilibrium steady states, Phys. Rev. Res. **1**, 033021 (2019).

[62] Y. Hasegawa, Quantum thermodynamic uncertainty relation for continuous measurement, Phys. Rev. Lett. **125**, 050601 (2020).

[63] T. Van Vu and K. Saito, Thermodynamics of precision in Markovian open quantum dynamics, Phys. Rev. Lett. **128**, 140602 (2022).

[64] K. Prech, P. Johansson, E. Nyholm, G. T. Landi, C. Verdozzi, P. Samuelsson, and P. P. Potts, Entanglement and thermokinetic uncertainty relations in coherent mesoscopic transport, Phys. Rev. Res. **5**, 023155 (2023).

[65] S. V. Moreira, M. Radaelli, A. Candeloro, F. C. Binder, and M. T. Mitchison, Precision bounds for multiple currents in open quantum systems, Phys. Rev. E **111**, 064107 (2025).

[66] G. Blasi, R. R. Rodríguez, M. Moskalets, R. López, and G. Haack, Quantum kinetic uncertainty relations in mesoscopic conductors at strong coupling, arXiv:2505.13200.

[67] D. Palmqvist, L. Tesser, and J. Splettstoesser, Kinetic uncertainty relations for quantum transport, arXiv:2410.10793.